

Synthesis and Ring-Opening Metathesis Polymerization of Aryl-Substituted 1,1'-(1,3-Butadienylene)ferrocenes

Richard W. Heo, Joon-Seo Park, and T. Randall Lee*

Department of Chemistry, University of Houston, 4800 Calhoun Road, Houston, Texas 77204-5003

Received October 21, 2004; Revised Manuscript Received December 21, 2004

ABSTRACT: The unsaturated aryl-substituted ferrocenophanes 1,1'-(1-phenylbuta-1,3-diene-1,4-diyl)ferrocene and 1,1'-(1-mesitylbuta-1,3-diene-1,4-diyl)ferrocene were synthesized and used to prepare high molecular weight conjugated polymers by ring-opening metathesis polymerization. X-ray crystal structures of the phenyl- and mesityl-substituted monomers showed substantial bond angle strain in the butadiene bridge. The monomers were readily polymerized upon exposure to a tungsten-based initiator to give high molecular weight polymers that were soluble in common organic solvents. UV/vis spectral analysis indicated that the aryl moieties gave rise to enhanced conjugation when compared to related alkyl-substituted ferrocene-containing polymers. The enhanced conjugation was further supported by electrochemical analysis. The thermal stability of the new ferrocene-containing polymers was similar to that of oligomeric poly(ferrocenylene), and the conductivities upon doping were on the order of 10^{-5} S cm^{-1} .

Introduction

Transition-metal-containing polymeric systems have been the subject of extensive study due to their unique electrical, magnetic, and optical properties.^{1–9} In particular, conjugated polymers that contain transition-metal backbones have received a great deal of interest because of their potential to combine the attractive electrical properties of metals with the strength, flexibility, and processability of organic polymers.² Among this class of materials, conjugated ferrocene-containing polymers are of considerable interest due to ferrocene's excellent thermal, redox, and spectroscopic properties.^{10–12} Previous efforts to synthesize these types of materials, however, have afforded insoluble oligomers or polymers that are poorly conducting and/or display electrochemical behavior similar to that of ferrocene.^{10,13–21} Furthermore, the insolubility of conjugated polymers with ferrocene-containing backbones has limited both their characterization and their capacity to be processed into useful device structures.⁶ The development, therefore, of a new strategy to tailor the microstructures of ferrocene-based polymers is critical to the development and use of these materials in device applications.

Poly(ferrocenylenes) with π -conjugated organic bridges are of particular interest because of the promising electronic, optical, and magnetic properties afforded by potential interactions of the iron centers through the π -network. To this end, many studies have targeted electron-delocalized polymers containing ferrocenylene groups linked directly together²² or linked by π -conjugated organic spacers such as vinylene,^{23–25} divinylene,²¹ phenylenevinylene,²⁶ phenyleneacetylene,²⁷ *p*-phenylene,²⁸ naphthylene,²⁹ heteroatomic thienylene,³⁰ and [2.2]paracyclophane.³¹ Unfortunately, most synthetic routes to these materials have typically afforded conjugated polymers with poor solubilities and low molecular weights.^{21,23–25} Grubbs and co-workers, for example, explored the ring-opening metathesis polymerization (ROMP) of 1,1'-(1,3-butadienylene)ferrocene

(**1**) (Figure 1), which gave marginally soluble low molecular weight oligomers.²¹ Similarly, Buretea and Tilley explored the ROMP of *ansa*-(vinylene)ferrocene (**2**) (Figure 1), which gave insoluble oligomers.²⁵ The poor solubility of both types of materials inhibited not only their characterization but also the ability to prepare them in high molecular weight form. Overcoming solubility limitations is thus essential before these and related materials can be widely studied and used.

Our more recent efforts utilizing the ROMP of strategically functionalized derivatives of **1** have provided a unique route to the synthesis of high molecular weight conjugated polymers with ferrocene units in the backbone.^{32–34} Specifically, the synthesis of 1,1'-(1-*tert*-butyl)-1,3-butadienylene)ferrocene (**3**) (Figure 1) followed by ROMP afforded poly(ferrocenylene-*tert*-butyldivinylene) having high molecular weights (e.g., $M_w > 300000$) and solubilities in many common organic solvents.^{32–34} The successful polymerization and the solubility of the resultant polymer are unprecedented for conjugated organometallic polymers having high molecular weights. While characterization of these materials by UV/vis spectroscopy showed extended conjugation upon polymerization,^{32–34} and electrochemical measurements showed electronic interactions between neighboring metal centers,³⁴ the electrical conductivities upon doping by I_2 were disappointing ($\sim 10^{-5}$ S cm^{-1}).³⁴

In the present study, we have targeted the synthesis of derivatives of **3** (and the corresponding polymers) in which the *tert*-butyl group is replaced by an aromatic group (**4** and **5** in Figure 1). We wished to incorporate aromatic moieties because we felt that these substituents might ultimately be used to enhance the electrical conductivity of the polymers by affording electrical tunability through selective substitution on the aromatic ring (e.g., by incorporating electron-donating substituents on the ring).³⁴ In this paper, we demonstrate that the aromatic groups phenyl and mesityl can be successfully attached to the 1-position of the 1,3-butadienyl bridge of 1,4-(1,1'-ferrocenediyl)-1,3-butadiene (**1**). Moreover, ROMP of the aryl-substituted monomers **4** and **5** affords high molecular weight polymeric materials that are soluble in organic solvents.

* To whom correspondence should be addressed. E-mail: trlee@uh.edu.

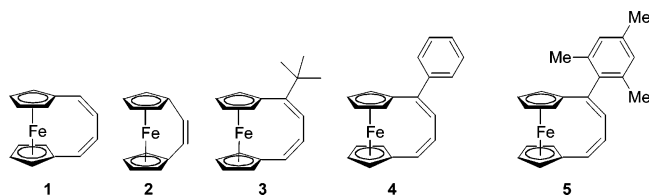


Figure 1. Ferrocenophanes used in ROMP trials.

Experimental Section

General Procedures. All chemical transformations were performed in Schlenk flasks under an inert atmosphere (N_2 or Ar) or in a nitrogen-filled Innovative Technologies glovebox, unless specified otherwise. Hydrocarbon solvents were dried by passage through alumina and then deoxygenated with a Cu-based catalyst (Q-5, Englehard) before use. A column of activated alumina was also used to dry ethereal and halogenated solvents. Degassing for all solvents was performed using freeze–pump–thaw cycles before use. Phenylmagnesium bromide (1.0 M solution in diethyl ether) and mesitylmagnesium bromide (1.0 M solution in THF) were purchased from Aldrich Chemicals, and packaged under nitrogen in Sure/Seal bottles. The tungsten-based initiator used in these studies, $W(=NPh)[=CHPh(2-OMe)][OC(CF_3)_2(CH_3)_2](THF)$, was prepared as reported by Grubbs and co-workers.³⁵

Monomer Syntheses. The monomers used in these studies, 1,1'-(1-phenylbuta-1,3-diene-1,4-diyl)ferrocene (**4**) and 1,1'-(1-mesitylbuta-1,3-diene-1,4-diyl)ferrocene (**5**), were synthesized via the key intermediate 1,1'-(4-oxobut-1-ene-1,4-diyl)ferrocene (**6**) (see Scheme 1), which was prepared using a route developed by Pudelski and Callstrom.³⁶

Synthesis of 1,1'-(4-Hydroxy-4-phenylbut-1-ene-1,4-diyl)ferrocene (7**).** A sublimated aliquot (0.50 g, 2.0 mmol) of **6** and a magnetic stirring bar were placed in a 100 mL Schlenk flask that was thoroughly dried under argon before use. After 60 mL of dry diethyl ether was transferred to this flask, 4.0 mL (4.0 mmol) of a solution of phenylmagnesium bromide (1.0 M in THF) was added dropwise via syringe at 0 °C. Upon addition, the solution turned noticeably darker. The reaction mixture was slowly allowed to warm to room temperature and stirred for an additional 2 h. After the mixture was washed with saturated NH_4Cl and brine, the organic phase was concentrated to afford a crude oily product, **7**. The crude products were purified by column chromatography on silica gel using 5% Et_2O in hexanes ($R_f = 0.13$) to give fine yellow crystals of **7** (0.40 g, 60% yield). 1H NMR (300 MHz, C_6D_6): δ 7.60 (d, $J = 7.8$ Hz, 2 H), 7.15 (t, $J = 7.8$ Hz, 2 H), 7.01 (t, $J = 7.8$ Hz, 1 H), 6.18 (d, $J = 7.8$ Hz, 1 H), 5.54–5.63 (m, 1 H), 3.71–4.32 (m, 8 H), 3.01 (dd, $J = 6.9, 13.2$ Hz, 1 H), 2.77 (dd, $J = 9.0, 13.2$ Hz, 1 H), 2.08 (s, 1 H). ^{13}C NMR (75 MHz, C_6D_6): δ 150.2, 129.5, 128.2, 127.2, 126.6, 125.6, 95.7, 81.2, 70.7, 69.2, 69.1, 68.9, 68.7, 68.3, 67.5, 66.8, 41.0.

Synthesis of 1,1'-(1-Phenylbuta-1,3-diene-1,4-diyl)ferrocene (4**).** 10-Camphorsulfonic acid (0.23 g, 1.0 mmol) was dissolved in 150 mL of benzene in a 200 mL round-bottomed flask equipped with a magnetic stirring bar and a reflux condenser. To this mixture was added dropwise a solution of recrystallized **7** (0.30 g, 0.90 mmol) in 30 mL of benzene. After the addition, the mixture was heated under reflux for 2 h, concentrated to 50 mL under reduced pressure, and dissolved in 100 mL of hexanes. The solution was washed with saturated NH_4Cl and brine, and removal of the volatiles afforded a dark solid material. The crude products were purified by column chromatography on silica gel using hexanes ($R_f = 0.42$) to give fine red needles of **4** (0.19 g, 68% yield). 1H NMR (300 MHz, C_6D_6): δ 7.28 (d, $J = 5.7$ Hz, 2 H), 7.15 (s, 1 H), 7.07 (d, $J = 5.7$ Hz, 2 H), 6.21 (d, $J = 12.3$ Hz, 1 H), 5.81 (d, $J = 5.7$ Hz, 1 H), 5.59 (dd, $J = 5.7, 12.3$ Hz, 1 H), 4.38 (d, $J = 27.3$ Hz, 4 H), 4.06 (d, $J = 27.3$ Hz, 4 H). ^{13}C NMR (75 MHz, C_6D_6): δ 145.1, 142.8, 129.5, 128.1, 127.6, 127.5, 127.3, 124.3, 81.1, 78.6, 70.6, 70.4, 69.6, 68.2.

Synthesis of 1,1'-(4-Hydroxy-4-mesitylbut-1-ene-1,4-diyl)ferrocene (8**).** An aliquot (0.50 g, 2.0 mmol) of **6** and a magnetic stirring bar were placed in a 100 mL Schlenk flask that was thoroughly dried under argon before use. After 70 mL of dry diethyl ether was transferred to this flask, the mixture was cooled to 0 °C. To the reaction mixture stirred at 0 °C was transferred dropwise 4.0 mL (4.0 mmol) of a solution of 2-mesitylmagnesium bromide (1.0 M in THF). Upon addition, the solution turned noticeably darker. The reaction mixture was slowly warmed to room temperature and stirred for an additional 2 h. The organic layer was washed with saturated NH_4Cl , and removal of the volatiles under vacuum afforded the crude oily product **8**. Chromatography on silica gel using 5% Et_2O in hexanes ($R_f = 0.13$) as the eluant afforded fine yellow crystals of **8** (0.40 g, 54% yield). 1H NMR (300 MHz, C_6D_6): δ 6.75 (s, 2 H), 6.26 (dd, $J = 1.5, 11.1$ Hz, 1 H), 5.56–5.65 (m, 1 H), 4.41 (dd, $J = 1.5, 3.3$ Hz, 1 H), 3.87–4.02 (m, 7 H), 3.41 (ddd, $J = 1.5, 8.4, 12.3$ Hz, 1 H), 3.03 (dd, $J = 8.4, 12.3$ Hz, 1 H), 2.52 (s, 6 H), 2.10 (s, 3 H), 1.81 (s, 1 H). ^{13}C NMR (75 MHz, C_6D_6): δ 143.2, 136.7, 135.4, 132.4, 129.5, 95.7, 81.2, 72.5, 70.2, 69.7, 69.6, 69.3, 69.2, 68.7, 67.8, 67.7, 43.4, 25.5, 20.4.

Synthesis of 1,1'-(1-Mesitylbuta-1,3-diene-1,4-diyl)ferrocene (5**).** A solution of 10-camphorsulfonic acid (0.23 g, 1.0 mmol) in 100 mL of benzene was prepared in a 200 mL round-bottomed flask equipped with a magnetic stirring bar and a reflux condenser. To this round-bottomed flask was added dropwise a solution of **8** (0.35 g, 0.94 mmol) in 20 mL of benzene. After the addition was completed, the reaction mixture was stirred under reflux for 2 h. The mixture was concentrated to 50 mL under reduced pressure and then dissolved in 100 mL of hexanes. The solution was washed with saturated NH_4Cl and brine, and the volatiles were removed under vacuum to afford a dark solid material. The crude product was purified by column chromatography on silica gel using hexanes ($R_f = 0.40$) to give fine red needles of **5** (0.21 g, 59% yield). 1H NMR (300 MHz, C_6D_6): δ 6.76 (s, 2 H), 6.22 (d, $J = 12.6$ Hz, 1 H), 5.44 (dd, $J = 12.6, 6.9$ Hz, 1 H), 5.35 (d, $J = 6.9$ Hz, 1 H), 4.61 (t, $J = 1.8$ Hz, 2H), 4.41 (t, $J = 1.8$ Hz, 2H), 4.05 (t, $J = 1.8$ Hz, 2H), 4.00 (t, $J = 1.8$ Hz, 2H), 2.38 (s, 6 H), 2.14 (s, 3 H). ^{13}C NMR (75 MHz, C_6D_6): δ 141.8, 136.1, 135.1, 129.3, 128.8, 127.2, 126.6, 81.4, 78.2, 70.2, 70.0, 68.0, 67.8, 21.0, 20.7.

X-ray Crystallography. All measurements were made with a Siemens SMART platform diffractometer equipped with a 1K CCD area detector. A hemisphere of data (1271 frames at a 5 cm detector distance) was collected using a narrow-frame method with scan widths of 0.30° in ω and an exposure time of 20 s/frame. The first 50 frames were measured at the end of data collection to monitor instrument and crystal stability, and the maximum correction on I was <1%. The data were integrated using the Siemens SAINT program, with the intensities corrected for Lorentz factor, polarization, air absorption, and absorption due to variation in the path length through the detector faceplate. A φ scan absorption correction was applied based on the entire data set. Redundant reflections were averaged. Final cell constants were refined using 5774 reflections having $I > 10\sigma(I)$, and these, along with other information pertinent to data collection and refinement, are listed in Table 1. The Laue symmetry was determined to be $2/m$, and from the systematic absences noted the space group was shown unambiguously to be $P2(1)/c$.

Polymer Synthesis and Purification. Polymerizations of **4** and **5** were conducted in 1 dram vials by dissolving the monomer (~10–200 equiv) and the catalyst (3–10 mg) separately in ~1–2 mL of either dried CH_2Cl_2 or benzene. The vials were capped to prevent solvent evaporation and stirred gently with a magnetic stirring bar. The progress of the polymerization was monitored by color and viscosity changes in the solution. The polymerizations were terminated by the addition of a few drops of benzaldehyde.²¹ Experimental details of a typical polymerization are provided. To a 1 dram vial equipped with a miniature stirring bar were added 3.0 mg (3.6×10^{-6} mol) of the tungsten initiator $W(=NPh)[=CHPh(2-OMe)][OC(CF_3)_2(CH_3)_2](THF)$ ³⁵ and ~1 mL of CH_2Cl_2 . To this solution

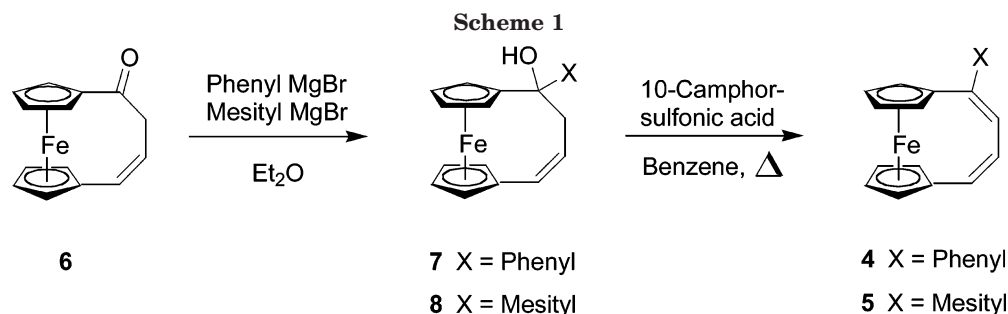


Table 1. X-ray Crystallographic Data and Structure Refinement for 1,1'-(1-Phenylbuta-1,3-diene-1,4-diyl)ferrocene (4) and 1,1'-(1-Mesitylbuta-1,3-diene-1,4-diyl)ferrocene (5)

	4	5
empirical formula	C ₂₀ H ₁₆ Fe	C ₂₃ H ₂₂ Fe
fw	312.18	354.26
dimensions (mm)	0.35 × 0.18 × 0.10	0.40 × 0.24 × 0.22
cryst syst	monoclinic	monoclinic
temp (K)	223(2)	223(2)
space group	P2(1)/c	P2(1)/c
a	8.968(1)	14.1201(6)
b	5.734(1)	15.7190(6)
c	28.003(3)	8.0672(3)
β	91.61(1)	105.144(1)
vol (Å ³)	1439.4(3)	1728.36(12)
Z	4	4
density(calcd) (g/cm ³)	1.441	1.361
abs coeff (mm ⁻¹)	1.037	0.872
R1	0.028	0.024
wR2	0.065	0.065

was added 0.13 g (3.6×10^{-4} mol) of **5** dissolved in CH₂Cl₂ (~2.5 mL). This mixture was sealed with a Teflon-lined cap to prevent solvent loss, and allowed to stir under nitrogen for 24 h. Benzaldehyde was added to terminate the polymerization.²¹ The solution was then added dropwise to a stirred solution of methanol (~30 mL), which afforded a red precipitate. After centrifugation and decanting of the supernatant, the precipitate was dissolved in CH₂Cl₂ (~5 mL), and then repeatedly precipitated into hexanes (~30 mL) until the supernatant became clear (typically four precipitations into hexanes). Removal of the volatiles afforded a dark powdery substance (0.06 g, 1.6×10^{-4} mol, 47% yield), identified as **10**. ¹H NMR (300 MHz, C₆D₆): δ 6.2–7.8 (br, 5 H), 3.8–4.6 (br, 8 H), 2.0–2.5 (br, 9 H). ¹³C NMR (75 MHz, C₆D₆): δ 141.8, 136.1, 135.8, 135.6, 135.1, 129.3, 128.8, 127.2, 126.6, 124.4, 85.5, 85.3, 85.2, 84.1, 83.4, 82.7, 78.6, 71.8, 71.9, 71.3, 70.2, 70.0, 68.0, 67.8, 20.9, 20.8, 20.7. Similarly, polymer **9** was obtained. ¹H NMR (300 MHz, C₆D₆): δ 6.9–7.6 (br, 5 H), 6.0–6.4 (br, 3 H), 4.0–4.6 (br, 8 H). ¹³C NMR (75 MHz, C₆D₆): δ br 140–145, 128.8, 127.8, br 80–90, br 68–74.

Analytical Measurements. ¹H and ¹³C NMR spectra were recorded on a General Electric QE-300 spectrometer at 300.2 and 75.5 MHz, respectively. All chemical shifts are reported relative to the residual proton or carbon signal of the deuterated solvents. A Varian Cary 3-Bio UV/vis spectrophotometer was used to collect ultraviolet/visible absorption spectra. The compounds were dissolved in THF or CH₂Cl₂ in a standard quartz cell, 1 × 1 × 4 cm³. The thermal stability of the polymers was evaluated using a TA Instrument Auto Hi-Res TGA 2950 thermogravimetric analyzer with a Thermal Solutions V 2.5 for Windows NT program for data manipulation. An aliquot of the polymer sample (~10 mg) was heated at 2.0 °C/min under a flow of N₂ gas, and the percent weight loss of the sample vs temperature was recorded. The differential scanning calorimetry (DSC) data were measured using a TA Instrument DSC 2010 in a sealed aluminum pan. The sample was heated from 50 to 250 °C at a rate of 10 °C/min under a flow of nitrogen. Conventional heat flow vs temperature was obtained using a Universal V2.5H TA Instruments program. Molecular weight analysis was performed using gel permeation

chromatography (GPC) on a Waters GPC system equipped with a Waters 510 pump, a 410 differential refractometer, and two Waters Styragel HR columns. THF was used as the eluant at a flow rate of 1.0 mL/min. Molecular weights were obtained using a calibration curve generated from narrow molecular weight polystyrene standards purchased from Polysciences. Polymer solutions (3–5 mg/mL) were filtered through 0.45 μm Millipore, Millex FH 13 mm filters before injection. Electrical conductivity was measured with a homemade four-point probe system, which has been described separately.³⁴

Spin-Casting and Doping of Thin Polymer Films. Polymer samples (20 mg) dissolved in benzene (1 mL) were filtered through 0.45 μm Millipore, Millex FH 13 mm filters before use. A glass substrate was placed on Headway Research spin-coater, and the polymer solution was cast dropwise onto the glass substrate. The films were spun dry and then further dried under vacuum. The polymer films were exposed to iodine vapor (200 mmHg) in an evacuated Schlenk flask for selected intervals of time (typically 2–5 h). Upon doping, the initially translucent red films became black. To ensure complete removal of any excess iodine, the sample was placed under vacuum for 30 min before measurements were taken.

Results and Discussion

Synthesis of 1,1'-(1-Phenylbuta-1,3-diene-1,4-diyl)ferrocene (4) and 1,1'-(1-Mesitylbuta-1,3-diene-1,4-diyl)ferrocene (5). The key intermediate in our strategy for synthesizing unsaturated aryl-substituted ferrocenophanes is the butenone-bridged ferrocenophane **6**, which was first reported by Pudelski and Callstrom.³⁶ As in our previous synthetic strategy to synthesize *tert*-butyl-substituted ferrocenophane **3**,^{32–34} we targeted carbon-1 (C-1) on the bridge of **6** as the site for the attachment of the pendant aryl group (see Scheme 1). Successful arylation of **6** was achieved by the use of the commercially available Grignard reagents phenylmagnesium bromide and mesitylmagnesium bromide to afford after dehydration ferrocenophanes **4** and **5** in 36% and 32% overall yield, respectively. After purification by column chromatography followed by recrystallization from ethanol/hexane, the resulting fine red needles of **4** and **5** were stable in air and soluble in common organic solvents, including hexane, benzene, methylene chloride, and tetrahydrofuran (THF). Crystals of **4** and **5** are dark red in color, while crystals of *tert*-butyl-substituted ferrocenophane **3** have an orange color, similar to that of ferrocene.³²

Single-Crystal X-ray Diffraction Analysis of 4 and 5. Compounds **4** and **5** were obtained as clear, dark red crystals, which were characterized by single-crystal X-ray diffraction (see Figure 2 and the Supporting Information). While the structures of **4** and **5** are similar to each other and to those of 1,1'-(1-methoxy-1,3-butadienylene)ferrocene³⁶ and the parent unsubstituted 1,1'-(1,3-butadienylene)ferrocene (**1**),³⁷ the structures are markedly different from that of 1,1'-(1-*tert*-butyl)-1,3-butadienylene)ferrocene (**3**).³² Table 2 gives selected

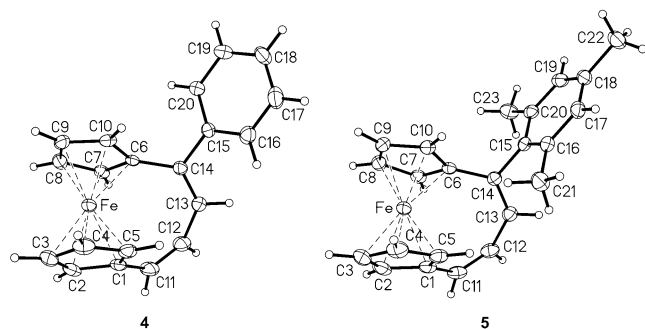


Figure 2. Thermal ellipsoid plots (40% probability level) of **4** and **5**.

Table 2. Selected Bond Distances (Å) and Bond Angles (deg) for Monomers **1**, **3**, **4**, and **5**

	1 ^a	3 ^b	4	5
Selected Bond Distances (Å)				
C11–C12	1.314	1.331	1.333	1.337
C12–C13	1.450	1.475	1.467	1.460
C13–C14	1.323	1.325	1.345	1.341
Selected Bond Angles (deg)				
C6–C14–C13	129.0	126.8	125.4	127.6
C12–C13–C14	130.7	136.8	132.9	131.9
C11–C12–C13	130.9	136.2	131.7	133.0
C1–C11–C12	128.5	131.6	128.1	125.2

^a From ref 37. ^b From ref 32.

bond angles for **1**,³⁷ **3**,³² **4**, and **5**. We note that, in **1**, **4**, **5**, and the methoxy-substituted monomer,³⁶ the cyclopentadienyl (Cp) rings are staggered and tilted with respect to each other. The dihedral angles between the Cp rings (i.e., the Cp-ring tilt angles) are 6.7°, 8.2°, 10.2°, and 7.2° and 11.1° for **1**, **4**, **5**, and the two independent molecules of 1,1'-(1-methoxy-1,3-butadienylene)ferrocene, respectively. In the *tert*-butyl-substituted monomer **3**, however, the Cp rings lie in a nearly eclipsed conformation and are roughly parallel, as indicated by a small 3.8° dihedral angle. Accordingly, the torsion angles of the butadiene bridges in monomers **4** and **5** are ca. 41.0° and ca. 40.1°, respectively, while that for monomer **1** is ca. 42° and that for the methoxy-substituted monomer ranges between 35° and 40°. These values are significantly larger than that found for the *tert*-butyl-substituted monomer **3** (ca. 2°).

It is important to evaluate the strain in unsaturated ferrocenophanes, given that ring strain is known to influence ROMP reactivity.²¹ Strain in ferrocenophanes can be evaluated on the basis of the Cp-ring tilt angle and/or the bond angle distortion in the butadiene bridge.³⁸ Table 2 shows the bond angle distortion of the heteroannular bridges of monomers **1**, **3**, **4**, and **5**. Importantly, the data show that there is considerable deviation from the ideal sp²-hybridized angle of 120° in both **4** and **5**. In particular, the interior pair of angles C(11)–C(12)–C(13) and C(12)–C(13)–C(14) are distorted to a greater extent than the exterior pair C(1)–C(11)–C(12) and C(6)–C(14)–C(13). This feature is also true for the parent unsubstituted ferrocenophane **1**³⁷ and the *tert*-butyl-substituted monomer **3**.³² The latter monomer, however, exhibits the largest distortion of all (the average C–C–C bond angle is 130° for **1**, 133° for **3**, 130° for **4**, and 129° for **5**). The larger bond angle distortion for **3** suggests that the *tert*-butyl-substituted monomer **3** is more strained than the unsubstituted monomer **1** and the aryl-substituted monomers **4** and **5**. On the other hand, monomer **3** exhibits a

smaller Cp-ring tilt angle than monomers **1**, **4**, and **5**, suggesting less strain for **3**. As a whole, the structural distinctness of **3** likely arises from the steric bulk of the *tert*-butyl group, which limits the torsion of the Cp rings, giving rise to small ring tilt strain but substantial bond angle strain in the bridge.

The distinct torsion angles of butadiene-bridged ferrocenophanes are reflected by the color of their crystals. For example, the unsubstituted monomer **1**, the methoxy-substituted monomer, and the aryl-substituted monomers **4** and **5** are all red in appearance. These monomers possess relatively large Cp-ring tilt angles and butadiene-bridge torsion angles, corresponding to an enhanced flexibility that allows the butadiene bridge to orient in a manner in which the π -orbitals of the bridge partially overlap with those of the Cp rings. This overlap gives rise to a bathochromic shift in the UV spectrum (vide infra) and contributes to the increased intensity of color for these monomers. In contrast, the *tert*-butyl-substituted monomer **3**, which possesses a small Cp-ring tilt angle (3.8°) and a small butadiene-bridge torsion angle (ca. 2°), is orange in appearance, perhaps even lighter in color than ferrocene. The relatively light color of **3** probably arises from an orthogonal orientation that the butadiene bridge is forced to adopt due to steric constraints imposed by the bulky *tert*-butyl group. This sterically constrained geometry permits little or no π -overlap between the butadiene bridge and the Cp rings.

The aryl substituents also uniquely influence the color of the monomer crystals. Monomer **4** is darker than both monomer **5** and the unsubstituted parent monomer **1**. We attribute this difference to π -conjugation between the phenyl substituent and the butadiene bridge. While the phenyl ring in monomer **4** is oriented to permit such π -conjugation, the methyl groups on the mesityl substituent in monomer **5** hinder the aryl group from orienting in such a manner to optimize overlap (see Figure 2). Similarly, no π -enhancement would be expected for the parent monomer **1**, given the absence of an aryl substituent.

Polymerization of 4 and 5. The strain in **4** and **5** apparent from the crystallographic data suggested to us that **4** and **5** are viable candidates for ROMP (see Scheme 2). Moreover, we anticipated that the solubility afforded by the aryl substituents³⁹ would facilitate the generation of high molecular weight polymers.³² Indeed, exposure of ferrocenophanes **4** and **5** to the highly reactive tungsten-based metathesis initiator W(=NPh)[=CHPh(2-OMe)][OC(CF₃)₂(CH₃)₂](THF)³⁵ shown in Scheme 2 afforded soluble conjugated polymers **9** and **10**, respectively. We monitored the polymerizations visually by noting that the initially red monomeric solutions turned deep red and became more viscous and opaque as the reaction proceeded. The polymerizations could be followed quantitatively by ¹H NMR spectroscopy (vide infra).

We terminated the polymerizations by adding benzaldehyde, which cleaves the polymer chain from the metal center.^{21,39} The polymers were precipitated into methanol and then repeatedly into hexanes and/or *n*-pentane from CH₂Cl₂. Unlike the polymer derived from the *tert*-butyl-substituted monomer **3**,³² polymers **9** and **10** were slightly soluble in hexanes and even *n*-pentane, which hindered their isolation from low molecular weight impurities.

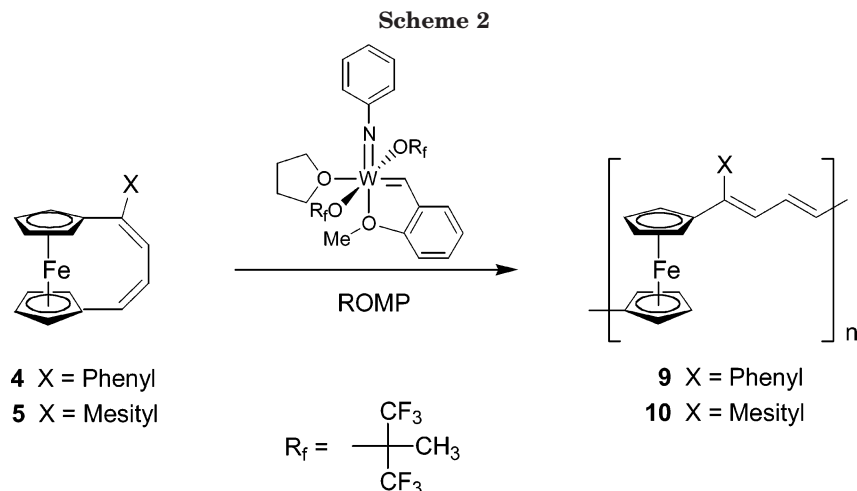


Table 3. Molecular Weight as a Function of the Monomer:Catalyst Ratio for Polymer 10

monomer: catalyst ratio	M_w	PDI ^a	monomer: catalyst ratio	M_w	PDI ^a
50:1	62000	1.73	150:1	74000	1.44
75:1	46000	1.87	200:1	70000	2.03
100:1	51000	2.16			

^a Polydispersity index.

Gel Permeation Chromatography (GPC). GPC analysis of polymers **9** and **10** revealed moderate molecular weights with relatively narrow weight distributions. To our surprise, the molecular weights failed to vary with the ratio of monomer to catalyst for both polymerizations (see, for example, the data in Table 3 for polymer **10**). Although we varied the amount of excess monomer added to a fixed quantity of catalyst, the molecular weights (M_w) for both polymers were always less than 100000. The observed molecular weights were lower than those that we obtained in analogous side-by-side trials using the *tert*-butyl-substituted monomer **3**, for which the molecular weights can be controlled by varying the monomer-to-catalyst ratio.^{32–34} For the aryl-substituted analogues, the lower molecular weights and the inability to vary the molecular weight by varying the monomer-to-catalyst ratio might arise from the fact that the strain in **4** and **5** is less than that in **3** (i.e., the difference in bond angle strain might be more important than the difference in ring tilt strain).^{32,34} Nevertheless, although the molecular weights of the polymers derived from **4** and **5** were routinely lower than those of the polymer derived similarly from **3**, the molecular weights reported here are still greater than those found for structurally similar π -conjugated organometallic polymers.^{21,23–30}

¹H and ¹³C Nuclear Magnetic Resonance (NMR) Spectroscopy. The ¹H NMR spectra of monomers **4** and **5** and the corresponding polymers **9** and **10** exhibited changes consistent with conversion of the monomers to polymers (Figure 3). After polymerization, for example, the ¹H NMR resonances broadened and shifted downfield. The downfield shift can be rationalized by an increase in electron delocalization for the polymer relative to that of the monomer.⁴⁰

The chemical shift difference between the H_α and H_β protons attached to the Cp rings of ferrocenophanes can be used to predict qualitatively the relative tilt of the Cp-ring planes with respect to each other.^{41,42} For the

nonbridged 1,1'-divinylferrocene, for example, the difference between these chemical shifts is 0.18 ppm.⁴³ In contrast, for the highly tilted *ansa*-(vinylene)ferrocene (**2**), the difference is 0.79 ppm.²⁵ By using this marker, we analyzed the chemical shifts of the Cp hydrogens in the ¹H NMR spectra of **4** and **5** (Figure 3) to provide an indirect measure of the ring tilt strain. We found that the chemical shift difference between the H_α and H_β protons in monomers **4** and **5** is 0.32 and 0.47 ppm, respectively, which is consistent with moderate ring tilt.^{41,42} Analysis of the monomers by X-ray crystallography (vide supra) provides firm support for this conclusion.

The ¹³C NMR spectra of monomers **4** and **5** and those of the corresponding polymers **9** and **10** exhibited resonances consistent with their proposed structures (see Figure 4). We assign the resonances between 65 and 75 ppm to the carbons of the Cp rings, and the

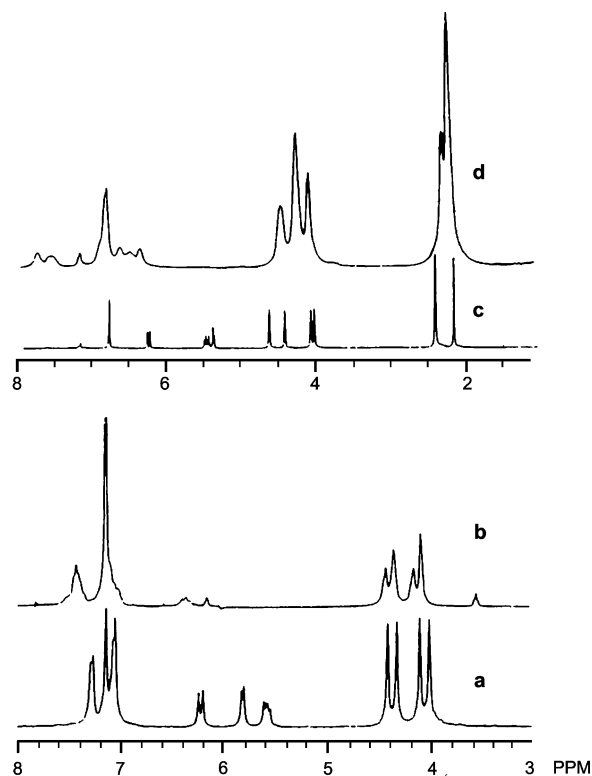


Figure 3. ¹H NMR spectra in C₆D₆ of (a) monomer **4**, (b) polymer **9** in which traces of monomer **4** remain, (c) monomer **5**, and (d) polymer **10** in which traces of monomer **5** remain.

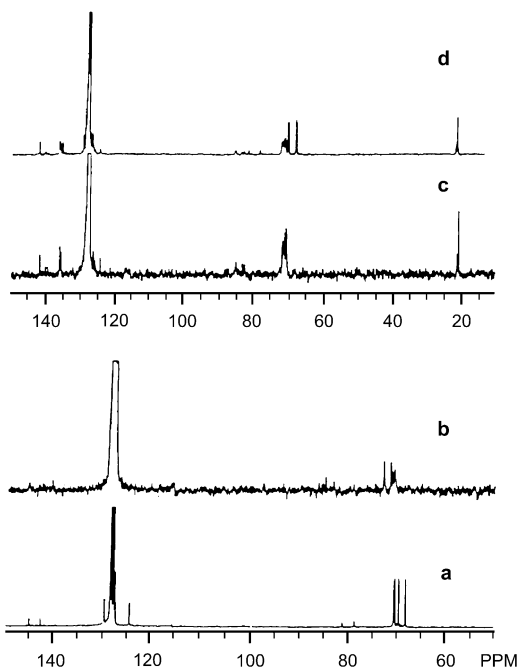


Figure 4. ^{13}C NMR spectra in C_6D_6 of (a) monomer **4**, (b) polymer **9**, (c) monomer **5**, and (d) polymer **10**.

resonances between 125 and 130 ppm to the olefinic carbons of the butadiene bridge and the aryl carbons.²¹ The resonances for the polymers were generally broader than those of the corresponding monomers. Moreover, the olefinic resonances were shifted slightly downfield for the polymers relative to the monomers, which is consistent with extended conjugation for the polymers relative to the monomers. The appearance of new peaks in the 132 ppm region of the spectra for polymers **9** and **10** indicates that there are repeat units other than butadienes, perhaps suggesting a random combination of head-to-tail and head-to-head/tail-to-tail polymerization of monomer units. Given that metathesis likely takes place preferentially at the unsubstituted double bonds of monomers **4** and **5**,^{39,44} the head-to-head polymerization would give a polymer in which the ferrocene units are separated by one unsubstituted olefin ($\text{Fc}-\text{CH}=\text{CH}-\text{Fc}$) and the tail-to-tail polymerization would give a polymer in which the ferrocene units are separated by a triolefin ($\text{Fc}-\text{C}(\text{Ar})=\text{CH}-\text{CH}=\text{CH}-\text{C}(\text{Ar})-\text{Fc}$).

Ultraviolet/Visible Spectroscopy. The UV/vis spectra of monomers **4** and **5** and their respective polymers **9** and **10** were recorded in CH_2Cl_2 over the range of 300–600 nm to examine the degree of electron delocalization. Analysis of the UV/vis spectra for the monomers and polymers revealed bathochromic shifts of λ_{max} and increased absorption intensities upon polymerization. For example, comparison of monomer **4** and polymer **9** ($M_w = 46000$, $\text{PDI} = 1.2$) in Figure 5 shows that $\lambda_{\text{max}} = 476$ nm for **4** and 485 nm for **9**. Monomer **4** exhibited moderately intense absorptions ($\epsilon = 2.3 \times 10^2 \text{ M}^{-1} \text{ cm}^{-1}$, $c = 6.7 \times 10^{-4} \text{ M}$), whereas polymer **9** exhibited stronger absorptions ($\epsilon = 1.6 \times 10^3 \text{ M}^{-1} \text{ cm}^{-1}$, $c = 6.3 \times 10^{-5} \text{ M}$). These observations are consistent with our previous studies of the analogous *tert*-butyl-substituted system,^{32,34} where the value of λ_{max} for the polymer was red-shifted relative to that of the monomer. The observed bathochromic shifts can be attributed to a moderate increase in conjugation upon polymerization, where the coplanarity of the olefinic bonds and the

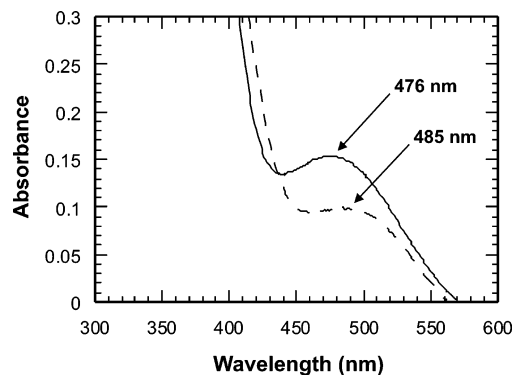


Figure 5. UV/vis spectra of monomer **4** (—, $6.7 \times 10^{-4} \text{ M}$) and polymer **9** (---, $6.3 \times 10^{-5} \text{ M}$).

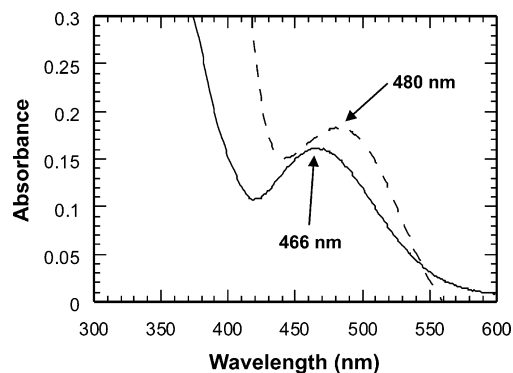


Figure 6. UV/vis spectra of monomer **5** (—, $6.4 \times 10^{-4} \text{ M}$) and polymer **10** (---, $7.1 \times 10^{-5} \text{ M}$).

adjacent Cp rings becomes more feasible. As noted above, visual inspection revealed that the initial solution of **4** exhibited a progressively deeper red color during polymerization, which is again consistent with an increase in conjugation.⁴⁵

Similar comparison of the mesityl-substituted monomer **5** ($\epsilon = 2.5 \times 10^2 \text{ M}^{-1} \text{ cm}^{-1}$, $c = 6.4 \times 10^{-4} \text{ M}$) and the corresponding polymer **10** ($M_w = 74000$, $\text{PDI} = 1.4$) ($\epsilon = 2.6 \times 10^3 \text{ M}^{-1} \text{ cm}^{-1}$, $c = 7.1 \times 10^{-5} \text{ M}$) also revealed an increase in absorption intensity upon polymerization. Moreover, the λ_{max} of monomer **5** at 466 nm exhibited an even larger bathochromic shift to 480 nm upon polymerization (Figure 6), which is again consistent with enhanced conjugation for the polymer relative to the monomer.⁴⁵

The Cp-ring tilt can also be evaluated by examining the λ_{max} values of the individual monomers; specifically, λ_{max} values typically undergo bathochromic shifts with increasing Cp-ring tilt.^{43,46} For example, Tilley's highly tilted **2** exhibits a λ_{max} value at 470 nm,²⁵ while ferrocene and 1,1'-dimethylferrocene show λ_{max} at 440 and 437 nm, respectively.^{41,47} Similarly, the slightly ring-tilted monomer **3** exhibits a λ_{max} at 444 nm,³⁴ which is slightly red-shifted from those of ferrocene and 1,1'-dimethylferrocene but blue-shifted from that of Tilley's monomer **2**. From these data, one can infer that monomer **3** possesses some degree of ring tilt strain but less than that of **2**, which is consistent with the X-ray data.³²

By comparison, monomers **4** and **5** show λ_{max} values of 476 and 466 nm, respectively. The λ_{max} value of the mesityl-substituted monomer **5** is clearly red-shifted from those of ferrocene, 1,1'-dimethylferrocene, and monomer **3** but only slightly blue-shifted from that of **2**, which can be interpreted to indicate that monomer **5**

possesses more ring tilt strain than monomer **3** but less than **2**. In contrast, the λ_{\max} value of monomer **4** is the most red-shifted of all. Given that the X-ray data show that the Cp rings of **2** are clearly more tilted than that of monomer **4** (vide supra), we can conclude that the ring tilt is not the only factor influencing the position of λ_{\max} . In particular, contributing π -orbital overlap from bridge substituents must be considered.

Comparison of the UV/vis spectra of monomers **3** ($\lambda_{\max} = 444$ nm),³⁴ **4** ($\lambda_{\max} = 476$ nm), and **5** ($\lambda_{\max} = 466$ nm) illustrates the effects of the substituent on orbital overlap. The *tert*-butyl-substituted monomer **3** exhibits the lowest value of λ_{\max} , which probably arises from the orthogonal orientation caused by the *tert*-butyl group and the lack of any π -interactions between the Cp rings and the butadiene bridge. However, the less bulky phenyl-substituted monomer **4** is sufficiently flexible to adopt an orientation that allows the phenyl group to lie in conjugation with the butadiene bridge, which leads to a large red shift in the value of λ_{\max} . In contrast, the mesityl-substituted monomer **5** is red-shifted relative to **3** but blue-shifted relative to **4**. For **5**, the methyl groups apparently hinder π -overlap between the aryl group and the butadiene bridge—a conclusion consistent with the crystallographic data (vide supra).

Comparison of the UV/vis spectra of the *tert*-butyl-substituted polymer ($\lambda_{\max} = 472$ nm),³⁴ polymer **9** ($\lambda_{\max} = 485$ nm), and polymer **10** ($\lambda_{\max} = 480$ nm) illustrates the effects of the substituents on the degree of conjugation of the polymers. The phenyl-substituted **9** and mesityl-substituted **10** exhibit slightly larger values of λ_{\max} than does the *tert*-butyl-substituted polymer. The aryl substituents can plausibly enhance the degree of conjugation relative to the *tert*-butyl substituent in one of two ways. First, the phenyl substituents might align themselves with the π cloud of the polymer backbone and thereby increase the degree of conjugation. Alternatively, the bulky *tert*-butyl group might lower the degree of conjugation by sterically inducing a twist in the polymer backbone. The fact that the value of λ_{\max} for the mesityl-substituted polymer falls between that of the other two suggests that perhaps both factors influence the degree of conjugation in polymer **10**.

Thermal Gravimetric Analysis (TGA) of Polymers 9 and 10. Examination of polymers **9** ($M_w = 46000$, PDI = 1.2) and **10** ($M_w = 74000$, PDI = 1.4) by TGA showed an onset of degradation at >350 °C for both polymers (Figure 7). Polymer **9** exhibited an onset of degradation at 360 °C with a relative residual weight of $\sim 50\%$ at 460 °C, reflecting its relatively high thermal stability. Similarly, polymer **10** exhibited an onset of degradation at 390 °C, which is slightly higher than that found for polymer **9**. Polymer **10** exhibited a relative residual weight of $\sim 40\%$ at 400 °C. The thermal decomposition behavior observed for these polymers is consistent with that reported for the structurally similar oligomeric poly(ferrocenylene).^{21,25,28} However, the enhanced thermal stability of polymers **9** and **10** compared to that of poly(*tert*-butyl-ferrocenylenedivinylene)³⁴ highlights the influence of substituents on the thermal stability of ferrocene-based conjugated polymers. A possible interpretation is that the aryl substituents stabilize the polymers via π -stacking interactions, especially at temperatures ≤ 350 °C.

Differential Scanning Calorimetry (DSC) of Polymers 9 and 10. Examination of polymers **9** ($M_w = 46000$, PDI = 1.2) and **10** ($M_w = 74000$, PDI = 1.4) by

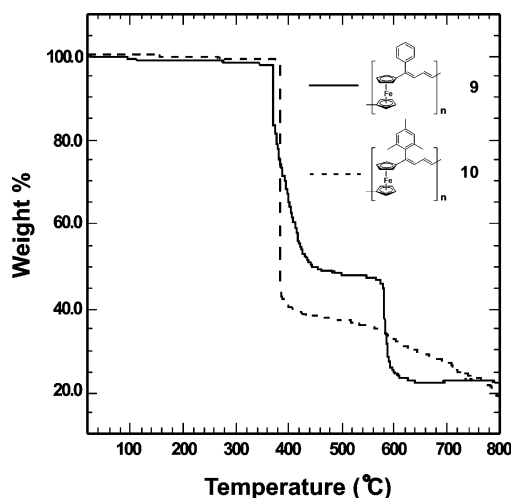


Figure 7. TGA plot obtained under nitrogen for polymers **9** and **10**.

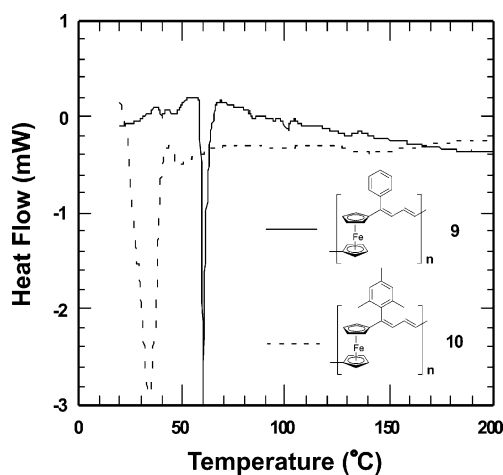


Figure 8. DSC plot obtained under nitrogen for polymers **9** and **10**.

DSC revealed no discernible endothermic transitions (Figure 8). Instead, both of these polymers exhibited distinct exothermic transitions in the range of 30–70 °C. Studies of the thermal phase behavior of structurally related aryl-linked poly(ferrocenylenes)²⁸ suggest that the exothermic transitions might be related to a recrystallization of the polymers. By comparison, the unsubstituted oligomeric poly(ferrocenylenebutenyne) exhibited no heat flow change until 385 °C,²¹ while structurally related derivatives of poly(1,1'-ferrocenylene-*alt-p*-oligophenylene) showed strong endothermic transitions at either 65 or 110 °C, depending on the length of the side chains.²⁸ Given these widely varying observations and the fact that the thermal phase behavior of polymers can be strongly influenced by the degree of crystallinity, minor differences in structure, and molecular weight, we conclude that the DSC data obtained here cannot be reliably compared to those obtained for other structurally related polymers.

Cyclic Voltammetry. We examined the electrochemistry of 1 mM solutions of monomers **4** and **5** and the corresponding polymers **9** and **10** in CH_2Cl_2 (Figure 9). Tetrabutylammonium hexafluorophosphate (TBAHFP) was used as the electrolyte in our experiments. The data were collected at a scan rate of 200 mV s⁻¹. Using solutions of ferrocene for reference, cyclic voltammograms of **4** and **5** showed single redox waves with peak-

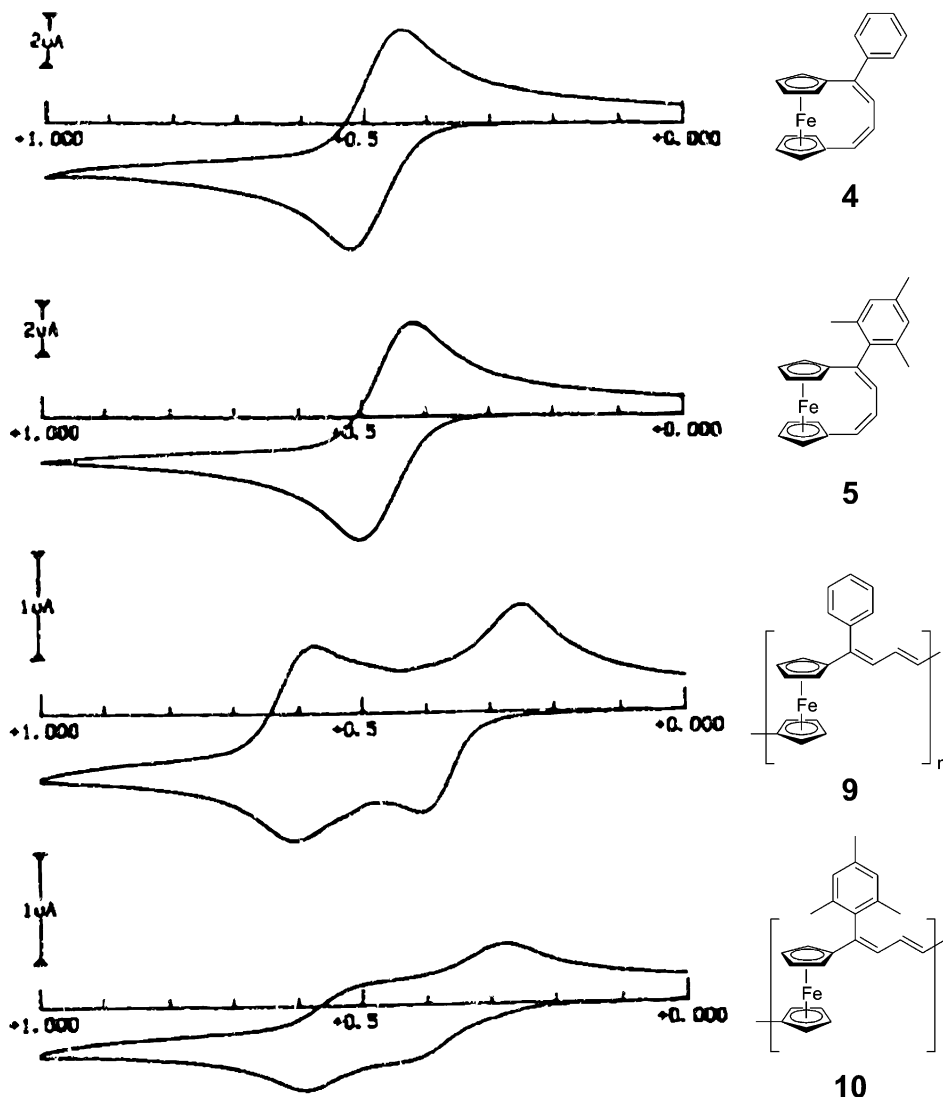


Figure 9. Cyclic voltammograms of 1 mM solutions of various samples in 0.1 M TBAHFP- CH_2Cl_2 : (from top to bottom) 1,1'-(1-phenylbuta-1,3-diene-1,4-diyl)ferrocene (**4**), 1,1'-(1-mesitylbuta-1,3-diene-1,4-diyl)ferrocene (**5**), poly(1,1'-((1-phenyl)-1,3-butadienyne)ferrocene) (**9**), and poly(1,1'-((1-mesityl)-1,3-butadienyne)ferrocene) (**10**).

to-peak separations of ~ 85 mV (Figure 9). The electrochemistry of **4** and **5** was observed to be completely reversible between potentials of 0.00 and +1.00 V vs the standard calomel electrode (SCE) at a scan rate of 200 mV s^{-1} . Monomer **4** exhibited an electrochemical potential of $E^\circ = 0.48$ V, while mesityl-substituted **5** exhibited an electrochemical potential of $E^\circ = 0.46$ V. For comparison, the electrochemical potential of ferrocene was found to be $E^\circ = 0.44$ V, and those for the unsubstituted parent ferrocenylenebutadiene **1** and the *tert*-butyl-substituted analogue **3** were found to be $E^\circ = 0.45$ V.^{21,34} Thus, the electrochemical potentials of the monomers were found to be similar to each other and to that of ferrocene. These measurements suggest that the butadiene bridge of the ferrocenophanes exerts no strong influence on the electrochemical potentials of the ferrocene center. This hypothesis is further supported by analysis of the ratio of the anodic peak current to the cathodic peak current of the molecules. At a scan rate of 200 mV s^{-1} , the ratio of the anodic peak current to the cathodic peak current was measured to be 0.99, 1.00, and 0.99 for ferrocene, monomer **4**, and monomer **5**, respectively.^{21,34}

Electrochemical methods were further used to probe the potential interactions between neighboring iron

centers in polymers **9** and **10** (see Figure 9). The cyclic voltammogram of polymer **9** ($M_w = 46000$, PDI = 1.2) shows two reversible redox waves with a separation of 260 mV. Similarly, the cyclic voltammogram of polymer **10** ($M_w = 74000$, PDI = 1.4) shows two reversible redox waves with a separation of 210 mV. These values along with the two-wave pattern are consistent with a chain possessing interacting metal centers.^{48–53} Polymers of noninteracting centers would show a single wave, as do the monomers described above.^{19,20} The separation between the two redox potentials (ΔE) is qualitatively representative of the magnitude of the interaction (as long as the relevant materials are closely related). For comparison, the polymer reported by Tilley²⁵ exhibits a ΔE value of 250 mV, and polymers reported by Manners⁴² exhibit ΔE values of 210–290 mV. These polymeric systems are all believed to possess interacting ferrocene nuclei.

The larger value of ΔE found for polymer **9** ($\Delta E = 260$ mV) compared to that found for polymer **10** ($\Delta E = 210$ mV) suggests that the electronic communication in polymer **9** is stronger than that in polymer **10**. Similarly, electrochemical studies of poly(*tert*-butylferrocenylene)divinylene revealed a completely reversible two-wave potential with a separation ΔE of 230 mV.³⁴ The

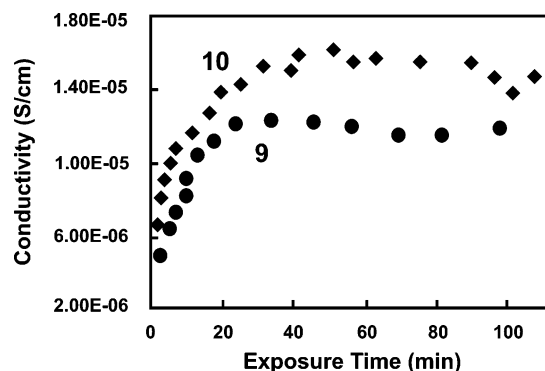


Figure 10. Vacuum conductivity of **9** and **10** as a function of the duration of exposure to I_2 vapor.

observed differences might arise from the ability of the phenyl-substituted polymer to adopt a favorable geometry that allows the greatest electronic communication (please see the above discussion regarding the UV/vis data).

Doping and Conductivity. Spin-coated samples of polymers **9** and **10** were dried under vacuum on a Schlenk line equipped with an attachment for introducing I_2 vapor. After drying, the highly resistive samples ($10^{11} \Omega$) were treated with ca. 200 mmHg of I_2 at ambient temperature. Instantly, the red translucent films became black. The conductivities were measured with respect to the doping time as described in the Experimental Section. Films of polymers **9** ($M_w = 46000$, PDI = 1.2) and **10** ($M_w = 74000$, PDI = 1.4) that were treated in this manner exhibited maximum conductivities on the order of $10^{-5} \text{ S cm}^{-1}$ (Figure 10). The measured conductivities are lower than those reported for either poly(ferrocenylenevinylene) ($10^{-3} \text{ S cm}^{-1}$)¹⁹ or poly(ferrocenylenedivinylene) ($10^{-4} \text{ S cm}^{-1}$).²⁰

It was our belief that incorporation of the aryl substituents would enhance the conductivity of **9** and **10** compared to that of the *tert*-butyl-substituted polymer by increasing the effective conjugation lengths of the polymers.³⁹ If, however, the major contributing mechanism of electronic conduction in these polymers is due to interchain hopping rather than intrachain conduction via the polymer backbone, incorporation of the aryl groups would be expected to have little or no effect upon the conducting properties. Since the UV/vis and electrochemical measurements suggest a greater conjugation length for polymer **9** than for either the *tert*-butyl-substituted polymer or polymer **10**, but the conductivity values are indistinguishable, the results obtained here suggest an interchain hopping mechanism of electrical conduction in these materials. We also note that the conductivities of the polymers failed to vary with changes in molecular weight (data not shown). These results further support the interchain hopping mechanism as the major mode of electron transport in these polymeric systems.

As a whole, however, the data reported here provide additional support that conjugated polymers with π -electron delocalization through ferrocenyl units are poorer electrical conductors than structurally related conjugated organic polymers.^{6,7} Recently, we described extended Hückel calculations that found an increased energy gap between the valence band and the lowest unoccupied band of poly(ferrocenylenedivinylene) when compared to polyacetylene.^{34,54} Thus, conjugated polymers having ferrocene units in the backbone should

exhibit lower conductivities than polyacetylene. This theoretical treatment and the experimental work described here, however, suggest that analogues of the aryl-substituted polymer **9** in which strong donor groups (e.g., dialkylamino) are substituted in the para position should possess a smaller band gap and thus an enhanced conductivity compared to polymer **9**. We are currently exploring the synthesis and study of these materials.

Conclusions

Polymers **9** and **10** were prepared via ROMP of monomers **4** and **5**, respectively. Even though the highest molecular weights of polymers **9** and **10** were lower than those of their *tert*-butyl-substituted cousin, the molecular weights were still higher than those of other previously studied poly(ferrocenylenes) with conjugated organic spacers. Bathochromic shifts in the UV/vis spectra of monomers **4** and **5** and polymers **9** and **10** compared to the *tert*-butyl-substituted analogues demonstrate enhanced conjugation due to overlap with the aromatic rings. Electrochemical studies of the polymers qualitatively support the UV/vis data by showing increased electronic interaction associated particularly with the phenyl-substituted polymer. For both **9** and **10**, cyclic voltammetry revealed two reversible oxidation waves. The presence of dual redox waves at distinct potentials ($\Delta E = 210\text{--}260 \text{ mV}$) suggests electronic communication between neighboring iron nuclei in the backbones of these polymers. The data further indicate slightly greater electronic communication in polymer **9** than in polymer **10**, which illustrates the important roles that both sterics and electronics play in dictating the electrochemical properties of these conducting polymers. The measured conductivities of iodine-doped samples of **9** and **10** failed to vary with molecular weight and fell within the semiconducting range ($10^{-5} \text{ S cm}^{-1}$). These data are consistent with a model in which interchain hopping is the dominant mechanism of electrical transport. The data are further consistent with previous extended Hückel calculations, which indicate that the ferrocene unit itself gives rise to the low conductivity by increasing the energy gap between the valence band and the conduction band.^{34,54} To decrease the band gap, future investigations will target the preparation and study of aryl-substituted poly(ferrocenylenedivinylene)s that incorporate strong donor groups on the aryl rings.

Acknowledgment. Generous support for this research was provided by the Robert A. Welch Foundation (Grant E-1320) and the Texas Institute for Intelligent Bio-Nano Materials and Structures for Aerospace Vehicles, funded by NASA Cooperative Agreement No. NCC-1-02038.

Supporting Information Available: X-ray crystallographic files in CIF format for monomers **4** and **5**. This material is available free of charge via the Internet at <http://pubs.acs.org>.

References and Notes

- (1) *Handbook of Conducting Polymers*; Skotheim, T. A., Ed.; Marcel Dekker: New York, 1986; Vols. 1 and 2.
- (2) Marks, T. J. *Science* **1985**, *227*, 881.
- (3) Mark, J. E.; Allcock, H. R.; West, R. *Inorganic Polymers*; Prentice Hall: Upper Saddle River, NJ, 1992.

- (4) *Inorganic and Organometallic Polymers II*; Wisian-Neilson, P., Allcock, H. R., Wynne, K. J., Eds.; ACS Symposium Series 572; American Chemical Society: Washington, DC, 1994.
- (5) Barlow, S.; O'Hare, D. *Chem. Rev.* **1997**, *97*, 637.
- (6) Manners, I. *Angew. Chem., Int. Ed. Engl.* **1996**, *35*, 1602.
- (7) Nguyen, P.; Gomez-Elipse, P.; Manners, I. *Chem. Rev.* **1999**, *99*, 1515.
- (8) Turner, M. L. *Annu. Rep. Prog. Chem., A.: Inorg. Chem.* **2001**, *97*, 443.
- (9) Gates, D. P. *Annu. Rep. Prog. Chem., A.: Inorg. Chem.* **2002**, *98*, 479.
- (10) Gooding, R.; Lillya, C. P.; Chien, C. W. *J. Chem. Soc., Chem. Commun.* **1983**, 151.
- (11) Scholl, H.; Sochaj, K. *Electrochim. Acta* **1991**, *36*, 689.
- (12) Cotton, F. A.; Wilkinson, G. *Basic Inorganic Chemistry*; Wiley: New York, 1987; p 622.
- (13) Arimoto, F. S.; Haven, A. C., Jr. *J. Am. Chem. Soc.* **1955**, *77*, 6295.
- (14) Chen, Y.-H.; Fernandez-Refojo, M.; Cassidy, H. G. *J. Polym. Sci.* **1959**, *40*, 433.
- (15) Pittman, C. U., Jr.; Lai, J. C.; Vanderpool, D. P.; Good, M.; Prado, R. *Macromolecules* **1970**, *3*, 746.
- (16) Neuse, E. W.; Rosenberg, H. *J. Macromol. Sci., Rev. Macromol. Chem.* **1970**, *C4* (1), 1.
- (17) Cowan, D. O.; Park, J.; Pittman, C. U., Jr.; Sasaki, Y.; Mukherjee, T. K.; Diamond, N. A. *J. Am. Chem. Soc.* **1972**, *94*, 5110.
- (18) Pittman, C. U., Jr.; Sasaki, Y.; Grube, P. L. *J. Macromol. Sci., Chem.* **1974**, *A8*, 923.
- (19) Smith, T. W.; Kuder, J. E.; Wychic, D. *J. Polym. Sci.* **1976**, *14*, 2433.
- (20) Flanagan, J. B.; Margel, S.; Bard, A. J.; Anson, F. C. *J. Am. Chem. Soc.* **1978**, *100*, 4248.
- (21) Stanton, C. E.; Lee, T. R.; Grubbs, R. H.; Lewis, N. S.; Pudelski, J. K.; Callstrom, M. R.; Erickson, M. S.; McLaughlin, M. L. *Macromolecules* **1995**, *28*, 8713.
- (22) Neuse, E. W.; Bednarik, L. *Macromolecules* **1979**, *12*, 187.
- (23) Itoh, T.; Saitoh, H.; Iwatsuki, S. *J. Polym. Sci., Part A: Polym. Chem.* **1995**, *33*, 1589.
- (24) Bayer, R.; Pöhlmann, T.; Nuyken, O. *Makromol. Chem., Rapid Commun.* **1993**, *14*, 359.
- (25) Buretea, M. A.; Tilley, T. D. *Organometallics* **1997**, *16*, 1507.
- (26) Gamble, A. S.; Patton, J. T.; Boncella, J. M. *Makromol. Chem., Rapid Commun.* **1993**, *13*, 109.
- (27) Morikita, T.; Maruyama, T.; Yamamoto, T.; Kubota, K.; Katada, M. *Inorg. Chim. Acta* **1998**, *269*, 310.
- (28) Knapp, R.; Velten, U.; Rehahn, M. *Polymer* **1998**, *39*, 5827.
- (29) Rosenblum, M.; Nugent, H. M.; Jang, K.-S.; Labes, M. M.; Cahalane, W.; Klemarczyk, P.; Reiff, W. M. *Macromolecules* **1995**, *28*, 6330.
- (30) Curtis, M. D.; Southard, G. E. *Organometallics* **1997**, *16*, 5618.
- (31) Morisaki, Y.; Chujo, Y. *Macromolecules* **2003**, *36*, 9319.
- (32) Heo, R. W.; Somoza, F. B.; Lee, T. R. *J. Am. Chem. Soc.* **1998**, *120*, 16.
- (33) Heo, R. W.; Lee, T. R. *Polym. Prepr. (Am. Chem. Soc., Div. Polym. Chem.)* **1998**, *39*, 169.
- (34) Heo, R. W.; Park, J.-S.; Goodson, J. T.; Claudio, G. C.; Takenaga, M.; Albright, T. A.; Lee, T. R. *Tetrahedron* **2004**, *60*, 7225.
- (35) Johnson, L. K.; Virgil, S. C.; Grubbs, R. H.; Ziller, J. W. *J. Am. Chem. Soc.* **1990**, *112*, 5384.
- (36) Pudelski, J. K.; Callstrom, M. R. *Organometallics* **1994**, *13*, 3095.
- (37) Erickson, M. S.; Fronczek, F. R.; McLaughlin, M. L. *Tetrahedron Lett.* **1993**, *34*, 197.
- (38) Stoeckli-Evans, H.; Osborne, A. G.; Whitely, R. H. *Helv. Chim. Acta* **1976**, *59*, 2402.
- (39) Gorman, C. B.; Ginsburg, E. J.; Grubbs, R. H. *J. Am. Chem. Soc.* **1993**, *115*, 1397 and references therein.
- (40) Elsenbaumer, R. L.; Jen, K.; Miller, G. G.; Eckhardt, H.; Shacklette, L. W.; Jow, R. In *Electronic Properties of Conjugated Polymer*; Kuzmany, H., Mehrring, M., Roth, S., Eds.; Springer-Verlag: Berlin, 1987; Vol. 76, pp 400–406.
- (41) Osborne, A. G.; Whiteley, R. H.; Meads, R. E. *J. Organomet. Chem.* **1980**, *193*, 345.
- (42) Manners, I. *Adv. Organomet. Chem.* **1995**, *37*, 131.
- (43) Rausch, M. D.; Siegel, A. *J. Organomet. Chem.* **1968**, *11*, 317.
- (44) Similar steric constraints have been observed in ring-closing metathesis (RCM) reactions: Kirkland, T. A.; Grubbs, R. H. *J. Org. Chem.* **1997**, *62*, 7310.
- (45) Scott, A. I. *Interpretation of the Ultra-Violet Spectra of Natural Products*; MacMillan: New York, 1964.
- (46) Butler, I. R.; Cullen, W. R.; Einstein, F. W. B.; Rettig, S. J.; Willis, A. J. *Organometallics* **1983**, *2*, 128.
- (47) Barr, T. H.; Watts, W. E. *J. Organomet. Chem.* **1968**, *15*, 177.
- (48) Brandt, P. F.; Rauchfuss, T. B. *J. Am. Chem. Soc.* **1992**, *114*, 1926.
- (49) Foucher, D. A.; Tang, B.-Z.; Manners, I. *J. Am. Chem. Soc.* **1992**, *114*, 6246.
- (50) Rulkens, R.; Lough, A. J.; Manners, I.; Lovelace, S. R.; Grant, C.; Geiger, W. E. *J. Am. Chem. Soc.* **1996**, *118*, 12683.
- (51) Nguyen, M. T.; Diaz, A. F.; Dement'ev, V. V.; Pannell, K. H. *Chem. Mater.* **1993**, *5*, 1389.
- (52) Nguyen, M. T.; Diaz, A. F.; Dement'ev, V. V.; Pannell, K. H. *Chem. Mater.* **1994**, *6*, 952.
- (53) The adsorption of ferrocene-containing polymers on electrodes can also give rise to two-wave patterns via the reduction of adsorbed polymers and the diffusion-controlled reduction of polymers in solution: Bard, A. J.; Faulkner, L. R. *Electrochemical Methods-Fundamentals and Applications*; Wiley: New York, 1980; Chapter 12.
- (54) The calculated band gap for poly(ferrocenylenedivinylene) was 1.8 eV, while that of polyacetylene was 0.7–0.9 eV.

MA047826W